

The quantum scattering time and its implications on scattering sources in graphene

X. Hong,¹ K. Zou,¹ and J. Zhu¹

¹*Department of Physics, The Pennsylvania State University, University Park, PA 16802*

(Dated: February 28, 2022)

We determine the quantum scattering time τ_q in six graphene samples with mobility of 4,400 $< \mu < 17,000$ cm²/Vs over a wide range of carrier density ($1.2 < n < 6 \times 10^{12}$ /cm²). τ_q derived from Shubnikov-de Haas oscillations ranges ~ 25 -74 fs, corresponding to a single-particle level broadening of 4.5-13 meV. The ratio of the transport to quantum scattering time τ_t/τ_q spans 1.5-5.1 in these samples, which can be quantitatively understood combining scattering from short-ranged centers and charged impurities located within 2 nm of the graphene sheet. Our results suggest that charges residing on the SiO₂ surface play a dominant role in limiting carrier mobility in current samples.

PACS numbers: 73.63.-b, 73.21.-b, 73.43.-f, 72.15.Lh

Understanding and eliminating extrinsic scattering sources in graphene is critical to the advancement of its fundamental study and technological applications. Despite many theoretical and experimental investigations into possible candidates, including charged impurities (CI), adsorbates, substrate corrugations, and ripples, contradictory observations remain and a clear picture has yet to emerge.^{1,2,3,4,5,6,7,8,9,10,11,12,13,14,15,16}

To date, most experimental studies have focused on probing the carrier mobility μ , or equivalently the transport scattering time $\tau_t = m^* \mu/e$.^{8,9,10,11,12,13,14,15} Another important parameter in two-dimensional (2D) transport, the quantum scattering time τ_q , has not been well studied. τ_q characterizes the momentum relaxation of a quasi-particle and relates to its quantum level broadening Γ through $\Gamma = \hbar/2\tau_q$.

Quantitatively, the difference between τ_q and τ_t in graphene is shown in the following equations:¹⁷

$$\begin{aligned} \frac{1}{\tau_q} &= \int_0^\pi Q(\theta)(1 + \cos\theta)d\theta \\ \frac{1}{\tau_t} &= \int_0^\pi Q(\theta)(1 + \cos\theta)(1 - \cos\theta)d\theta. \end{aligned} \quad (1)$$

Here, θ is the scattering angle and $Q(\theta)$ depends on specific scattering mechanisms.^{17,18} While small-angle events weigh heavily towards τ_q , τ_t is mostly affected by right angle scatterings. Measurement of τ_t/τ_q has proven to be a powerful diagnostic tool in revealing complex scattering scenarios in conventional 2D electron gases (2DEGs).^{18,19,20,21} For example, short-ranged scattering sources give rise to $\tau_t/\tau_q \sim 1$ while charged impurities far away from a 2DEG lead to predominately small-angle events, resulting in large τ_t/τ_q . The former has been observed in silicon inversion layers and the latter characterizes modulation doped GaAs 2DEGs.^{18,19,20} Despite its demonstrated importance, the study of τ_q in graphene has been scant. Existing data are largely obtained from the linewidth of cyclotron resonance at low densities.²² A systematic comparison between τ_t and τ_q has not been made.

In this work, we report a comprehensive study of τ_q in six graphene samples over a wide range of carrier

densities $1.2 < n < 6 \times 10^{12}$ /cm² and mobility 4,400 $< \mu < 17,000$ cm²/Vs. τ_q is obtained from Shubnikov-de Haas (SdH) oscillations and ranges approximately 25-74 fs in these samples, corresponding to $\Gamma = 4.5$ -13 meV. The n -dependence of τ_t , τ_q , and their ratio τ_t/τ_q can all be explained by a self-consistent Boltzmann transport theory^{3,17} using three parameters: the charged impurity density n_{imp} , the impurity-graphene distance z , and the resistivity from short-ranged scatterers ρ_{short} . Our results indicate that the mobility in current graphene-on-SiO₂ samples is limited by scattering from charges residing within 2 nm of the graphene sheet. We speculate that charges present at the graphene/SiO₂ interface are the major sources of scattering.

Single-layer graphene sheets are mechanically exfoliated onto 290 nm SiO₂/doped Si substrates and identified optically. Rectangular pieces are processed into Hall bar devices using standard e-beam lithography followed by metal deposition (Fig. 1 inset). The fabrication details are given in Ref.²³. Representative data from four samples (denoted as samples A-D) are presented in details.

Transport experiments are performed in a pumped He⁴ cryostat with a base temperature of 1.4 K and equipped with a 9 T magnet. Standard lock-in techniques are used with an excitation current of 50-200 nA. The doped Si substrates serve as back gate electrodes, to which a voltage (V_g) is applied to tune the carrier density and hence the conductance of graphene. We extract carrier density from SdH oscillations and obtain a gating efficiency of $\alpha = dn/dV_g = 7 \times 10^{10}$ /cm²V of the backgate. All measurements are taken at $T < 10$ K to eliminate electron-phonon scattering.

Figure 1 shows the conductivity σ vs V_g taken on samples A-D. $\sigma(V_g)$ varies linearly with V_g for the whole density range in sample A and exhibits sublinear $\sigma(V_g)$ at high V_g for samples B-D, where the "bowing" is most pronounced in sample C. The qualitative features of these traces resemble results reported previously,^{10,11,12,13} and have been explained by a self-consistent Boltzmann theory combining scattering from long and short-ranged

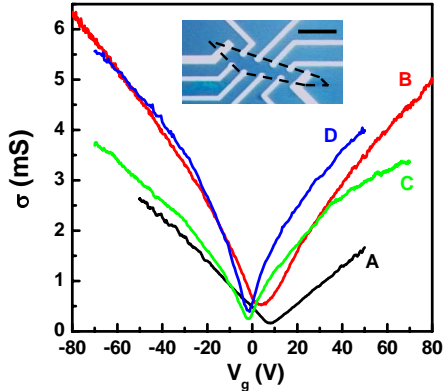


FIG. 1: (Color online) $\sigma(V_g)$ of samples A (black), B (red), C (green), and D (blue) below 10 K. Inset: Optical image of sample A. Edge of the piece outlined. Scale bar is 10 μm .

	μ_{FE} (cm^2/Vs)	ρ_{short} (Ω)	τ_q (fs)	τ_t/τ_q	z (nm)	n_{imp} ($10^{11}/\text{cm}^2$)
A	4,400	40	31(38)	2.7(2.2)	0	10.4
B	10,000	55	33(49)	5.1(3.4)	2(1)	(7.7)
C	9,500	165	66	1.7	0	4.8
D	17,000	105	53	3.5	2	7

TABLE I: μ_{FE} , ρ_{short} , τ_q , τ_t/τ_q , z , and n_{imp} for samples A-D. τ_q and τ_t/τ_q are given for $n \sim 3 \times 10^{12}/\text{cm}^2$. The uncertainty in z is 1-2 \AA for all samples. Data in parenthesis are after the corrections of density inhomogeneity.

sources:^{1,2,3}

$$\frac{1}{\sigma} = \frac{1}{\sigma_{\text{long}}} + \rho_{\text{short}}; \quad \sigma_{\text{long}} = ne\mu_{\text{FE}} + \sigma_{\text{res}}. \quad (2)$$

In this framework, ρ_{short} denotes a constant contribution to resistivity from short-ranged scattering sources such as defects or neutral adsorbates. CI are thought to give rise to a linear $\sigma(V_g)$, which implies a constant field effect mobility μ_{FE} and consequently $\tau_t \propto \sqrt{n}$. Equations 2 produce excellent fittings to the $\sigma(V_g)$ data of all our samples. The resulting μ_{FE} and ρ_{short} span 4,400-17,000 cm^2/Vs and 40-165 Ω respectively (Table I), covering much of the variations reported in the literature. The residue conductivity σ_{res} ranges 0.1-0.35 mS.^{12,24} In samples exhibiting electron-hole asymmetry, our analyses focus on the carrier type with the higher μ_{FE} to avoid complications associated with contact doping.²⁵

Although Eqs. 2 provide a good description of existing conductivity measurements, the origin of scattering sources in graphene is still under debate. In addition to CI, ripples, resonant scatterers and midgap states are also potential candidates.^{4,5,6,7} Unlike potassium adatoms,¹² certain adsorbates seem to dope graphene but not degrade its mobility.⁹ The role of the dielectric environment also appears controversial.^{13,14,15} While Jang *et al.* find agreement with the model using ice as a top dielectric layer,¹³ Ponomarenko *et al.* report screening effects much smaller than expected from the CI model using

liquid dielectric layers.¹⁵ Within the charged-impurity model, the origin of such impurities remain unclear: Adsorbates on top of graphene, charges adsorbed/trapped at the graphene/SiO₂ interface or residing inside the substrate are all possible candidates.

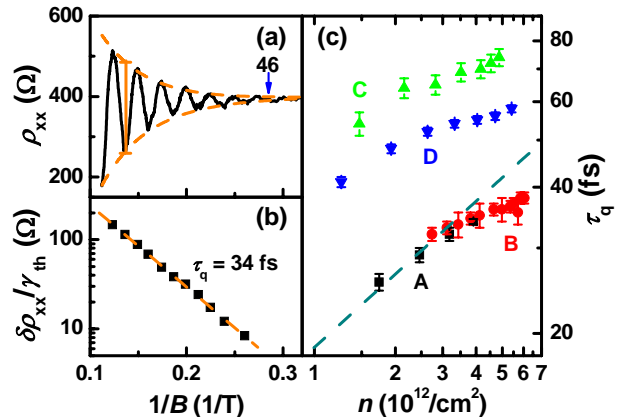


FIG. 2: (Color online) (a) $\rho_{xx}(1/B)$ of sample A at 1.6 K and $n = 3.89 \times 10^{12}/\text{cm}^2$. The onset of the oscillations corresponds to filling factor $\nu = 46$ (arrow). The vertical bar marks $2\delta\rho_{xx}$ at $\nu = 22$. The dashed lines correspond to Eqs. 3 with $\tau_q = 34$ fs. (b) The corresponding Dingle plot: $\delta\rho_{xx}/\gamma_{th}$ vs. $1/B$. τ_q is extracted from the linear fit. (c) $\tau_q(n)$ of samples A (squares), B (circles), C (up-triangles), and D (down-triangles) on a log-log plot. The dashed line indicates \sqrt{n} dependence.

We have measured the quantum scattering time τ_q in graphene to further address the above issues. We determine τ_q from the magnetic field dependence of SdH oscillations following procedures well-established in conventional 2DEGs.²⁰ Figure 2(a) shows the magnetoresistance $\rho_{xx}(B)$ of sample A at $n = 3.89 \times 10^{12}/\text{cm}^2$ and $T = 1.6$ K. The oscillatory amplitude $\delta\rho_{xx}$ can be described by:

$$\frac{\delta\rho_{xx}}{\rho_0} = 4\gamma_{th}\exp\left(-\frac{\pi}{\omega_c\tau_q}\right); \quad \gamma_{th} = \frac{2\pi^2k_B T/\hbar\omega_c}{\sinh(2\pi^2k_B T/\hbar\omega_c)}. \quad (3)$$

Here ρ_0 is the non-oscillatory background resistance, γ_{th} is the thermal factor, and ω_c the cyclotron frequency in graphene. Here $m^* = E_F/v_F^2 = \hbar\sqrt{\pi n}/v_F$ is the effective mass and $v_F = 1 \times 10^6$ m/s is the Fermi velocity in graphene. Figure 2(b) plots $\delta\rho_{xx}/\gamma_{th}$ vs. $1/B$ in a semi-log plot (the Dingle plot), where we extract $\tau_q = 34$ fs from the slope of the linear fit. The corresponding $\delta\rho_{xx}$ calculated from Eqs. 3 is plotted in Fig. 2(a) as dashed lines and exhibits excellent agreement with data. In each sample, the same procedure is repeated at different densities for $n > 1.2 \times 10^{12}/\text{cm}^2$, where several well-developed SdH oscillations are observed before the onset of quantum Hall states. In some traces, a slowly varying background is subtracted before the determination of $\delta\rho_{xx}$, as described in Ref.²³.

Figure 2(c) plots $\tau_q(n)$ in samples A-D (also listed in Table I for $n = 3 \times 10^{12}/\text{cm}^2$). $\tau_q(n)$ increases with increasing n in all samples and spans 25-74 fs for

$1.2 \times 10^{12}/\text{cm}^2 < n < 6 \times 10^{12}/\text{cm}^2$. These values correspond to a quantum level broadening $\Gamma = 4.5\text{-}13$ meV and are in line with $\Gamma = 20\text{-}30$ meV extracted from the adsorption linewidth of cyclotron resonances at $n < 1 \times 10^{12}/\text{cm}^2$.²²

The n -dependence of τ_q in Fig. 2(c) agrees qualitatively with that of $\sigma(V_g)$ in Fig. 1. This can be seen by separating the long and short-ranged components in $\tau_{t,q}$ using the following equations:¹⁷

$$\frac{1}{\tau_{t,q}} = \frac{1}{\tau_{t,q}^{\text{long}}} + \frac{1}{\tau_{t,q}^{\text{short}}}; \quad (4)$$

$$\tau_t^{\text{short}} = \frac{m^*}{ne^2\rho_{\text{short}}}; \quad \frac{\tau_t^{\text{short}}}{\tau_q^{\text{short}}} = 1.1.$$

Due to a small ρ_{short} , both τ_t and τ_q in sample A follow closely the \sqrt{n} dependence expected for charged impurities residing in the graphene plane ($z = 0$).¹⁷ Large ρ_{short} and higher μ_{FE} in samples B-D (Table I) cause both scattering times to deviate from the \sqrt{n} dependence. However, τ_q does not correlate with μ_{FE} in a simple relation. Samples B and C exhibit similar μ_{FE} , but their τ_q differ by a factor of 2. Samples A and B show comparable τ_q s despite the significant difference in μ_{FE} . Sample C, with a moderate μ_{FE} and the highest ρ_{short} , exhibits the highest τ_q .

To understand the above observations, we calculate the ratio $\tau_t/\tau_q(n)$ and the long-ranged component $\tau_t^{\text{long}}/\tau_q^{\text{long}}(n)$ using Eqs. 4, and plot the results in Figs. 3 (a) and (b) (also Table I). Samples A and B show n -independent τ_t/τ_q of 2.7 and 5.1 respectively. For the other two samples, τ_t/τ_q decreases slightly with increasing n , varying from 1.9 to 1.5 in sample C and 4.3 to 3.3 in sample D. Clearly, the angular distribution $Q(\theta)$ in Eqs. 1 differs significantly in these samples.

By evaluating $\tau_t^{\text{long}}/\tau_q^{\text{long}}(n)$, we find that such variation may be naturally explained by varying the impurity-graphene distance z within the charged-impurity model. Theoretical calculations of short and long-ranged ratios are given in solid and dashed lines, respectively, in Figs. 3 (a) and (b).^{3,17} According to this model, the $\tau_t^{\text{long}}/\tau_q^{\text{long}}(n)$ of sample A provides further evidence for the domination of CI located in the graphene plane ($z = 0$), where a constant 2.5 is expected (dashed line).^{3,17} The $\tau_t/\tau_q(n)$ in sample C falls between the dashed and solid lines, which is the result of a large short-ranged component. Its $\tau_t^{\text{long}}/\tau_q^{\text{long}}(n)$ exhibits an approximate constant ratio of 2.1, also pointing to CI located in the graphene plane (Fig. 3(b)). $\tau_t^{\text{long}}/\tau_q^{\text{long}}$ in samples B and D range from 5-7 and are best described by CI located 2 nm away from the graphene sheet (Fig. 3(b)). In all six samples, we find $2 < \tau_t^{\text{long}}/\tau_q^{\text{long}} < 7$, corresponding to CI located within 2 nm of the graphene sheet.

The knowledge of the impurity-graphene distance z is essential in correctly determining the CI density n_{imp} in the vicinity of graphene. In the CI model, n_{imp} is related to μ_{FE} through $\mu_{\text{FE}} = C/n_{\text{imp}}$, where $C = 5 \times 10^{15}/V\text{s}$ is

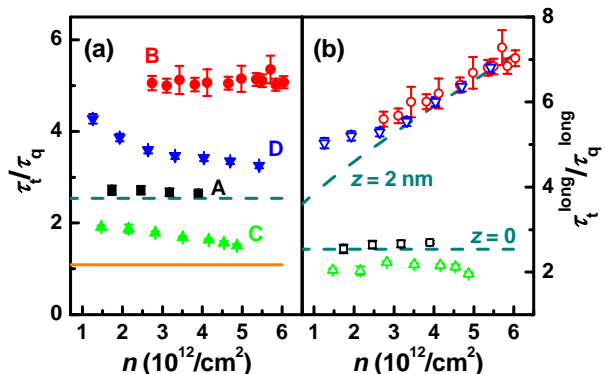


FIG. 3: (Color online) (a) τ_t/τ_q vs. n in samples A (squares), B (circles), C (up-triangles), and D (down-triangles) along with calculations for CI at $z = 0$ (dashed line) and δ -scattering centers (solid line) (¹⁷). (b) Their long-ranged component $\tau_t^{\text{long}}/\tau_q^{\text{long}}$ vs. n in corresponding open symbols. Dashed lines are calculations for $z = 0$ (bottom) and 2 nm (top) (¹⁷).

n -independent for $z = 0$.¹² At a finite z , C increases with increasing n due to screening. Using the equations in Refs.^{3,17}, we numerically calculate $C(n, z)$ and estimate n_{imp} by fitting $\sigma(n)$ to Eq. 2. The results are listed in Table I while an exemplary fitting is given in Ref.²³. Clearly, μ_{FE} (or τ_t) is affected by both z and n_{imp} . For example, the difference in μ_{FE} between samples A and D mainly stems from z , instead of n_{imp} . In contrast, τ_q serves as a better measure of n_{imp} due to its weaker dependence on z .

Next we briefly assess the effect of density inhomogeneity δn on the measurement of τ_q . Caused by CI, δn measures approximately a few $10^{11}/\text{cm}^2$ near the Dirac point,^{16,26} and is expected to decrease with increasing n due to electron screening.²⁷ δn introduces phase smearing in $\rho_{\text{xx}}(B)$, effectively reducing the SdH oscillation amplitude and suppressing the value of τ_q determined through the Dingle plot, as demonstrated in GaN 2DEGs.²¹ We have used the intercept of the Dingle plot at $1/B = 0$ as a criterion²⁰ to obtain δn and the corresponding corrections to τ_q . Details are given in Ref.²³. We estimate δn to be $\sim 7 \times 10^{10}/\text{cm}^2$ in sample A, and $\sim 9 \times 10^{10}/\text{cm}^2$ in sample B. These estimates are consistent with the highest filling factors observed in these samples ($\nu = 46$ for sample A and $\nu = 74$ for sample B). Overall, $\delta n/n$ decreases rapidly with n , in agreement with theory; but the magnitude is only a few percent in the density range we studied, which is significantly smaller than the theoretical predictions.^{23,27,28} The above correction leads to $\sim 20\%$ increase of τ_q in sample A and 50% in sample B. The corrected τ_q s are given in Table I in parenthesis. In samples C and D, the corrections are smaller than the error bars of τ_q and therefore omitted. $\tau_t^{\text{long}}/\tau_q^{\text{long}}$ in sample B now corresponds to CI located at $z = 1$ nm instead of previously determined $z = 2$ nm, but the main picture does not change.²³

Our study of τ_q and τ_t/τ_q provides critical information in differentiating various scattering scenarios in

graphene.^{4,5,6,7,17} A detailed comparison to theory is only made for the CI model at this point, but can be extended to other proposals as quantitative predictions become available. The diverse behavior our samples exhibit can all be understood very well within the CI model using three parameters: n_{imp} , z , and ρ_{short} . We speculate that uncontrolled spatial variation of SiO₂ surface properties, as well as sample preparation conditions (e. g. humidity) may have been the primary reasons behind the observed differences among samples, although variations in preparation procedures cannot be ruled out.²³

Our results indicate that the dominant CI reside within 2 nm of, and sometimes in the immediate vicinity of the graphene sheet. Primary candidates of this nature are charges carried by adsorbates on top of graphene and/or at the graphene/SiO₂ interface. The role of adsorbates is especially highlighted in the current annealing treatment of suspended graphene.^{10,11} In the literature, various approaches, including resist-free processing,^{16,29,30} UHV baking,^{13,16} and current annealing,³¹ have been used to remove contaminants on top of graphene without significant improvement to mobility. These observations collectively suggest that adsorbates on top of graphene cannot be the major culprit in limiting mobility at the current level. Instead, we speculate that charges (e. g. Na⁺) and molecular groups (e. g. OH) adsorbed/trapped on the SiO₂ surface prior to the exfoliation of graphene are the major source of scattering. The $z = 0$ found in samples A and C lends strong support to this hypothesis. Moreover, the small z observed in other samples can be accounted for by the existence of a spacer layer between graphene and SiO₂ (e.g. H₂O). The evidence of such a layer is widely observed in AFM height measurements of graphene. In this scenario, the concentration of adsorbed

charges (n_{imp}), together with the thickness of the spacer layer (z) can account for the wide span of mobility seen in our samples. It may also explain why graphene on a variety of substrates displays a similar range of mobility¹⁵ since the bulk properties of these substrates are less relevant here.

Finally we note that the above determined z can be expanded to represent an average impurity-graphene distance. Using this concept, we consider the contribution of uniformly distributed charges within the bulk of the SiO₂ substrate. Our simulations show that oxide charges in commercially available SiO₂ are unlikely to be a major source of scattering at the current mobility level.²³

In conclusion, we have systematically studied the quantum and transport scattering times in graphene. Our data will prove useful in critical examinations of existing scattering scenarios. Within the CI model, the ratio of τ_t/τ_q indicates that charged impurities residing within 2 nm of the graphene sheet are the main sources of scattering in graphene. Such information provides important guidance to the effort of improving carrier mobility in graphene.

Acknowledgments

We are grateful for helpful discussions with S. Adam and L. Song, and technical assistance from S.-H. Cheng and S. Syed. We thank P. Eklund for providing access to his Raman spectrometer. Work at Penn State is supported by NSF Grants No. ECS-0609243, No. CAREER DMR-0748604, and No. MRSEC DMR-0820404. The authors acknowledge use of facilities at the PSU site of NSF NNIN.

¹ T. Ando, J. of the Phys. Soc. of Japan **75**, 074716 (2006).

² K. Nomura and A. H. MacDonald, Phys. Rev. Lett. **98**, 076602 (2007).

³ S. Adam, E. H. Hwang, V. M. Galitski, and S. Das Sarma, Proc. Nat. Acad. Sci. U.S.A. **104**, 18392 (2007).

⁴ T. O. Wehling, A. V. Balatsky, M. I. Katsnelson, A. I. Lichtenstein, K. Scharnberg, and R. Wiesendanger, Phys. Rev. B **75**, 125425 (2007).

⁵ T. Stauber, N. M. R. Peres, and F. Guinea, Phys. Rev. B **76**, 205423 (2007).

⁶ M. I. Katsnelson and A. K. Geim, Phil. Trans. R. Soc. A **366**, 195 (2008).

⁷ M. I. Katsnelson, F. Guinea, and A. K. Geim, Phys. Rev. B **79**, 195426 (2009).

⁸ Y. W. Tan, Y. Zhang, K. Bolotin, Y. Zhao, S. Adam, E. H. Hwang, S. Das Sarma, H. L. Stormer, and P. Kim, Phys. Rev. Lett. **99**, 246803 (2007).

⁹ F. Schedin, A. K. Geim, S. V. Morozov, E. W. Hill, P. Blake, M. I. Katsnelson, and K. S. Novoselov, Nat. Mater. **6**, 652 (2007).

¹⁰ K. I. Bolotin, K. J. Sikes, Z. Jiang, M. Klima, G. Fudenberg, J. Hone, P. Kim, and H. L. Stormer, Solid State

Commun. **146**, 351 (2008).

¹¹ X. Du, I. Skachko, A. Barker, and E. Andrei, Nat. Nanotechnol. **3**, 491 (2008).

¹² J. H. Chen, C. Jang, S. Adam, M. S. Fuhrer, E. D. Williams, and M. Ishigami, Nat. Phys. **4**, 377 (2008).

¹³ C. Jang, S. Adam, J. H. Chen, E. D. Williams, S. Das Sarma, and M. S. Fuhrer, Phys. Rev. Lett. **101**, 146805 (2008).

¹⁴ X. Hong, A. Posadas, K. Zou, C. H. Ahn, and J. Zhu, Phys. Rev. Lett. **102**, 136808 (2009).

¹⁵ L. A. Ponomarenko, R. Yang, T. M. Mohiuddin, M. I. Katsnelson, K. S. Novoselov, S. V. Morozov, A. A. Zhukov, F. Schedin, E. W. Hill, and A. K. Geim, Phys. Rev. Lett. **102**, 206603 (2009).

¹⁶ Y. Zhang, V. W. Brar, C. Girit, A. Zettl, and M. F. Crommie, Nat. Phys. **5**, 722 (2009).

¹⁷ E. H. Hwang and S. Das Sarma, Phys. Rev. B **77**, 195412 (2008).

¹⁸ S. Das Sarma and F. Stern, Phys. Rev. B **32**, 8442 (1985).

¹⁹ J. P. Harrang, R. J. Higgins, R. K. Goodall, P. R. Jay, M. Laviron, and P. Delescluse, Phys. Rev. B **32**, 8126 (1985).

- ²⁰ P. T. Coleridge, *Phys. Rev. B* **44**, 3793 (1991).
- ²¹ S. Syed, M. J. Manfra, Y. J. Wang, R. J. Molnar, and H. L. Stormer, *Appl. Phys. Lett.* **84**, 1507 (2004).
- ²² Z. Jiang, E. A. Henriksen, L. C. Tung, Y. J. Wang, M. E. Schwartz, M. Y. Han, P. Kim, and H. L. Stormer, *Phys. Rev. Lett.* **98**, 197403 (2007).
- ²³ See EPAPS Document No. E-PRBMDO-80-R32948 for supporting information.
- ²⁴ M. Trushin and J. Schliemann, *Phys. Rev. Lett.* **99**, 216602 (2007).
- ²⁵ B. Huard, N. Stander, J. A. Sulpizio, and D. Goldhaber-Gordon, *Phys. Rev. B* **78**, 121402(R) (2008).
- ²⁶ J. Martin, N. Akerman, G. Ulbricht, T. Lohmann, J. H. Smet, K. Von Klitzing, and A. Yacoby, *Nat. Phys.* **4**, 144 (2008).
- ²⁷ E. Rossi and S. Das Sarma, *Phys. Rev. Lett.* **101**, 166803 (2008).
- ²⁸ M. Polini, A. Tomadin, R. Asgari, and A. H. MacDonald, *Phys. Rev. B* **78**, 115426 (2008).
- ²⁹ N. Staley, H. Wang, C. Puls, J. Forster, T. N. Jackson, K. McCarthy, B. Clouser, and Y. Liu, *Appl. Phys. Lett.* **90**, 143518 (2007).
- ³⁰ C. O. Girit and A. Zettl, *Appl. Phys. Lett.* **91**, 193512 (2007).
- ³¹ J. Moser, A. Barreiro, and A. Bachtold, *Appl. Phys. Lett.* **91**, 163513 (2007).